Preprints (www.preprints.org) | NOT PEER-REVIEWED | Posted: 13 May 2021 doi:10.20944/preprints202105.0282.v1

Design Optimization of Centrifugal Microfluidic "Lab-on-a-Disc" Systems towards Fluidic Larger-Scale Integration

Jens Ducrée

School of Physical Sciences, Dublin City University, Ireland

Abstract

Enhancing the degree of functional multiplexing while assuring operational reliability and manufacturability at competitive costs are crucial components to enable comprehensive sample-to-answer automation, e.g., for use in common, decentralized “Point-of-Care” or “Point-of-Use” scenarios. This paper demonstrates a model-based ‘digital twin’ approach which efficiently supports the algorithmic design optimization of exemplary centrifugo-pneumatic (CP) dissolvable-film (DF) siphon valves towards larger-scale integration (LSI) of well-established “Lab-on-a-Disc” (LoaD) systems. Obviously, the spatial footprint of the valves and their upstream laboratory unit operations (LUOs) have to fit, at a given radial position prescribed by its occurrence in the assay protocol, into the locally available disc space. At the same time, the retention rate of rotationally actuated valve and, most challenging, its band width related to unavoidable experimental tolerances need to slot into a defined interval of the practically allowed frequency envelope. A set of design rules, metrics, and methods and instructive showcases for computationally assisted optimization of valve structures are presented.

Introduction

Empowering even untrained operators to autonomously perform decentralized testing of bioliquids outside specialized laboratory infrastructure, such as hospital labs, general practitioners’ offices, in the field, or even at home represents the key driver for the development of so-called “Point-of-Care” (PoC) / “Point-of-Use” (PoU) devices. While immunochromatographic devices based on lateral flow, e.g., familiar from blood glucose or pregnancy testing, have been around for several decades, aging populations, the rise of chronic and life-style related diseases correlating with increasing age, wealth, nutritional habits and sedentary lifestyles of global populations, or recent pandemic threats, create the strong need for frequent, simple, reliable, cost-efficient and user-friendly monitoring of biochemical indicators in different body fluids.

Since their emergence the early 1990s [1], microfluidic Lab-on-a-Chip technologies, often quasi synonymously referred to as micro Total Analysis Systems (“µTAS”), have been touted a highly promising candidate to provide compact and inexpensive devices offering full sample-to-answer automation of multiplexed bioassay protocols [2, 3]. Manifold platform technologies have been established in the meantime, which might be categorized by their pumping, valving, actuation or detection schemes. The field has substantially diversified in the meantime, and many, mostly specialized solutions, have been successfully advanced to viable products.

Due to their plain concept of flow control by a simple spindle motor and its analogies to, at the time, booming optical data storage technologies such as CD and DVD, centrifugal microfluidic systems [4-33] have been one of the earliest microfluidic platforms to be developed starting around the mid-

 doi:10.20944/preprints202105.0282.v1

1990s; interestingly, these “Lab-on-a-Disc” (LoaD) systems, which conceptually resemble conventional centrifugal analyzers, were first commercialized before finding their way into academia around the turn of the millennium. By now, a huge global cohort of companies and research groups is involved in advancing and maturing LoaD technologies.

Note that, for the sake of simplicity, we use the term “disc” throughout this paper; however, a plethora of geometries, e.g., minidiscs, segments or microscope slides, which substantially deviate from the standard format of conventional optical data storage media displaying 12-cm (outer), 1.5 cm (inner hole) diameter and 1.2-mm thickness, have been introduced. Furthermore, different mounting concepts to the axis of rotation have been implemented. Yet, centrifugal flow control only scales with the radial position and the (square of the) spin rate, while not depending on the particular shape of the carrier chip and its mode of attachment to the spindle.

By virtue of the ubiquitous and unidirectional centrifugal field acting simultaneously on all liquids loaded to their potentially fast spinning device, valving concepts play a prominent role in LoaD technologies. While there have been active modes of control, e.g., by co-rotating pumps [34, 35] or sacrificial barriers [36, 37] opened by stimuli delivered by instrument mounted units, rotationally actuated schemes have attracted particular attention due to their smooth alignment with the simple and robust concept of LoaD platform with a rugged instrument “playing” a mostly single-use disc cartridge.

In traditional valving mechanisms, the spinning-induced pressure head acting on all disc-based liquid volumes is opposed by different sources of counterpressure. For instance, interfacial tension is at the root of capillary burst valves, and liquid in siphons are retained until the capillary action exceeds the centrifugal pressure by lifting [10], lowering [5] or accelerating [38] the spin rate across critical thresholds, or overflow prompted by volume addition under prevalent artificial gravity conditions. In most LoaD platforms, these valves retain the liquid during so-called laboratory unit operations (“LUOs”) such as particle sedimentation, metering and mixing are performed prior to detection in the final step of a bioanalytical protocol.

This work runs along the example of centrifugo-pneumatic (CP) dissolvable-film (DF) siphon valving that has shown to offer wide tunability, configurability, and operational robustness compared to other rotationally controlled valving schemes [39]. Yet, the portrayed approach can readily be extended to other flow control mechanisms. While essential ingredients for LoaD applications, we refer to various to the broad literature on centrifugally implemented LUOs and downstream detection techniques [14-33].

This paper investigates systematic design optimization of rotationally actuated valves to facilitate fluidic large(r)-scale integration (LSI), a notion first elaborated in the early 2000s in the context of pneumatically controlled elastomeric systems [40]. Based on previous work on ‘digital twin’ [41] modelling of fluidic performance and operational robustness [39, 42], valve retention frequencies and their band widths as key performance indicators of the LoaD systems can directly be calculated from the standard deviation of elementary input parameters, such as general (linear) machining and pipetting tolerances [43, 44].

These statistical spreads can either be found in manuals or the literature, or be determined by low-complexity test structures; importantly, these fluctuations are broadly independent of the specific layout of a specific LoaD cartridge. This method is hence essential to predict and optimize device performance and its operational robustness *in-silico*, prior to the time- and resource-consuming, and thus risky and costly development of manufacturing and assembly.

Preprints (www.preprints.org) | NOT PEER-REVIEWED | Posted: 13 May 2021 doi:10.20944/preprints202105.0282.v1

At first, the principles of centrifugal flow control are modelled to support a digital twin of LoaD systems orchestrated by a group of CP-DF siphon valves. Then, fundamental requirements underlying rotational valving for fluidic LSI in real and frequency space are elaborated. In the next section, a set of performance metrics supporting the initial, knowledge-based qualitative design and its subsequent computational optimization are defined. Examples for typical tasks in multiplexing and resulting valve geometries are given before compiling general rules guiding to the layout of multi-step / multi-reagent bioanalytical assay panels.

Rotational Flow Control

Pressures

A (contiguous) fluid segment of volume U_0 and density ϱ possessing a radial extension $\Delta r = r - r_0$ and mean radial position $\bar{r} = 0.5 \cdot (r + r_0)$ between its inner and outer menisci r and r_0, respectively, residing in a valve of (static) geometry Γ experiences a centrifugal pressure head

$$p_\omega = \varrho \cdot \bar{r} \Delta r \cdot \omega^2 \tag{1}$$

when spinning at an angular frequency $\omega = 2\pi \cdot \nu$. Given typical experimental values, e.g., $\varrho = 10^3\ \mathrm{kg\ m^{-3}}$, $\bar{r} = 3\ \mathrm{cm}$, $\Delta r = 1\ \mathrm{cm}$, lower and upper range spin rates $\nu = \omega/2\pi = 10\ \mathrm{Hz}$ and $50\ \mathrm{Hz}$, equation (1) yields $p_\omega \approx 12\ \mathrm{hPa}$ and $300\ \mathrm{hPa}$, respectively. So even the larger value of p_ω amounts to only about one third of the standard atmospheric pressure $p_{\mathrm{std}} = 1013.25\ \mathrm{hPa}$.

Additional pressures $p_\rightarrow$ and $p_\leftarrow$ may act on the fluid, which are directed parallel or against the main z-axis of a channel, respectively. The pneumatic pressure

$$p_V = p_0 \cdot \frac{V_0}{V} \tag{2}$$

results from the compression of an original gas volume V_0 initially held at ambient pressure p_0 to V (law of Boyle-Mariotte). Theoretically, p_V (2) can be made randomly large through sufficiently shrinking the end volume V (for fixed V_0). Note that, in addition to the compressibility, a volume-pressure relationship akin to (2) can also arise in fluidic systems containing flexible solid elements such as elastic membranes or lids. p_0 may also be modified by heating of cooling according to $V \propto T$ (Charles's law).

The capillary pressure

$$p_\Theta = \frac{4\sigma}{D} \cdot \cos\Theta \tag{3}$$

is exerted on a liquid of surface tension σ with a contact angle Θ to a (round) channel of diameter D. For water with $\sigma \approx 72.8 \times 10^{-3}\ \mathrm{N\ m^{-1}}$, and a hydrophobic contact angle $\Theta \approx 120°$ in a channel of diameter $D = 100\ \mu\mathrm{m}$, the capillary counterpressure amounts to $|p_\Theta| \approx 15\ \mathrm{hPa} \ll p_{\mathrm{std}}$, only, which would be matched by rather low spin rates in the region $\nu = \omega/2\pi \approx 10\ \mathrm{Hz}$. In refined models, also pressures resulting from deceleration of flow or inertial agitation of liquid samples and reagents driven by $r \cdot d\omega/dt$ ought to be factored in.

In hydrostatic equilibrium

$$p_\omega + p_\rightarrow = p_\leftarrow \tag{4}$$

a liquid distribution Λ stabilizes within a given geometry Γ in response to p_ω (1), $p_\rightarrow$ and $p_\leftarrow$, e.g., p_V (2) or p_Θ (3). The outer meniscus $r = r(\omega)$ is a function of ω, and r_0 can then be directly calculated for a given Γ and U_0.

Preprints (www.preprints.org) | NOT PEER-REVIEWED | Posted: 13 May 2021 doi:10.20944/preprints202105.0282.v1

Critical Spin Rate

During retention of rotationally actuated valves, the outer meniscus of Λ at $r(\omega)$ remains upstream of a critical filling level marked by a position in Γ. In case $p_{\rightarrow}$ and $p_{\leftarrow}$ do not (explicitly) depend on ω, combining (1) and (4) leads to a retention rate

$$\Omega = \Omega(U_0, \Gamma, z = Z) = \sqrt{\frac{p_{\leftarrow} - p_{\rightarrow}}{\varrho \cdot \bar{r} \Delta r}} \tag{5}$$

beyond which the liquid is released at $\omega > \Omega$ and $\omega < \Omega$ for high- and low-pass valves, respectively. For the sake of clarity, we focus on high-pass valves in the following.

Example: Centrifugo-Pneumatic Siphon Valves

In prior publications, we have compared different rotationally actuated valving schemes for LoaD systems through a more general digital twin approach [39, 42]. It turns out that normally-closed centrifugo-pneumatic (CP) siphon valves with a compression chamber of volume V_C that is initially sealed by dissolvable-film (DF) membrane offer many operational benefits; amongst them are high tunability of the critical spin rate Ω (5), high operational robustness, and wide configurability in real as well as the frequency domain.

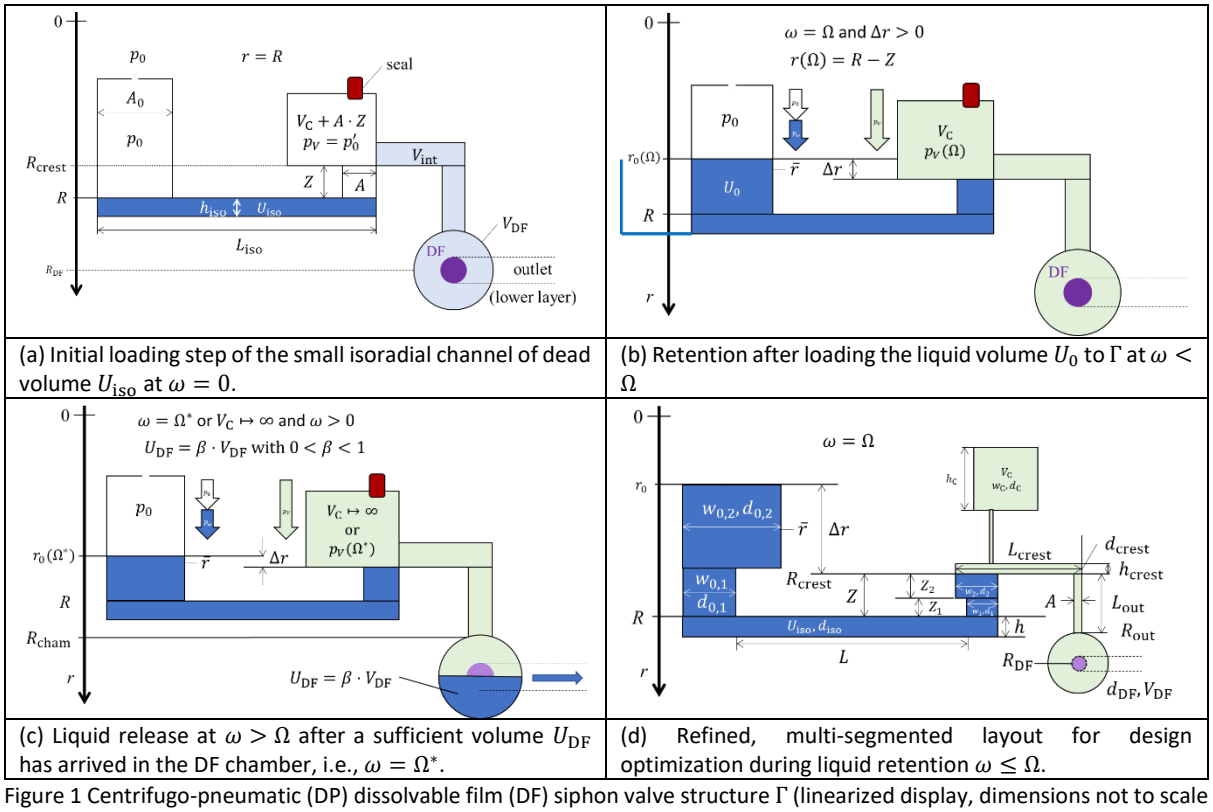

(a) Initial loading step of the small isoradial channel of dead volume U_{iso} at $\omega = 0$.

(b) Retention after loading the liquid volume U_0 to Γ at $\omega < \Omega$

(c) Liquid release at $\omega > \Omega$ after a sufficient volume U_{DF} has arrived in the DF chamber, i.e., $\omega = \Omega^*$.

(d) Refined, multi-segmented layout for design optimization during liquid retention $\omega \leq \Omega$.

Figure 1 Centrifugo-pneumatic (DP) dissolvable film (DF) siphon valve structure Γ (linearized display, dimensions not to scale with typical measures listed in the Appendix). The depth of all components upstream of the crest point amounts to 1 mm, and 200 µm thereafter. (a) In a first step, a liquid volume U_{iso} is loaded to the basic structure Γ which pneumatically isolated the inlet reservoir that is open to atmosphere at p_0 from the downstream compression chamber. E.g., due to dynamic effects, the actual pressure p_0' in the enclosed volume might (slightly) deviate from p_0. (b) The liquid volume $U_0 \gg U_{iso}$ is retained upstream of the crest point at $R_{crest} = R - Z$ for spin rates $\omega < \Omega$. (c) The high-pass CP-DF siphon valve opens for $\omega > \Omega^* \approx \Omega$ upon arrival of a minimum volume U_{DF} in the DF chamber. (d) Multi-segmented version for illustrating the key geometrical features for design optimization according to a given set of metrics.

Figure 1 illustrates the basic operating principle of CP-DF siphon valving structure Γ located at a basic radial position R from the axis of rotation. In a (hypothetical) priming procedure, a liquid volume U_{iso} is first loaded to the tiny isoradial channel; as a result, a gas volume V_0 composed of a main

Preprints (www.preprints.org) | NOT PEER-REVIEWED | Posted: 13 May 2021 doi:10.20944/preprints202105.0282.v1

compression chamber of volume $V_{C,0}$, an inbound segment of volume $A \cdot Z$, and tiny outlet features with negligible volume contributions $V_{out}/V_0 \ll 1$ is cut off from the inlet that is open to atmospheric at p_0 (Figure 1a, typical dimensions in the Appendix). The actual pressure p_0' in the enclosed gas might deviate from the ambient pressure p_0, e.g., due to filling dynamics. Then, the remainder of U_0 is added to the open inlet reservoir. At the retention rate $\omega = \Omega$, the outer meniscus has progressed in the radially inbound section of cross section A and axial length Z to the crest point at $R_{crest} = R - Z$ (Figure 1b).

This high-pass, CP-DF siphon valve opens above $\omega = \Omega$ when sufficient liquid U_{DF} has entered into the outer chamber to cover the local DF membrane at R_{DF} (Figure 1c). Strictly speaking, there is a release rate $\Omega^* > \Omega$ needed for displacing U_{DF} from the inbound section terminated at R_{crest} into the outer chamber to open the valve. This offset is usually very small and can be calculated from (5) by substituting U_0 by $U_0' = U_0 - U_{DF}$; for the sake of clarity, we assume $\Omega^* \approx \Omega$. Figure 1d displays a multi-segmented design of the basic structure Γ used later for refined optimization.

Inserting $p_{\rightarrow} = p_0$ and $p_{\leftarrow} = p_V$ (2), we obtain

$$\Omega = \sqrt{\frac{p_0 \cdot (V_C/V - 1)}{\varrho \cdot \bar{r} \Delta r}} \tag{6}$$

for the critical retention rate Ω (5) of CP-DF siphon valves with $V = V_C - A \cdot Z$.

Operational Robustness

The critical frequencies Ω (5, 6) of a rotationally controlled valves depend on a number of parameters $\{\gamma_i\}$, such as the loaded liquid volume U_0 (its density ϱ is fairly constant for aqueous solutions at room temperature), the structural dimensions of Γ, and the quantities determining the relevant pressure contributions. Experimentally, each γ_i is thus subject to a spread of normal distribution exhibiting a standard deviation $\Delta\gamma_i$. Consequently, also the resulting critical spin rate Ω (5) displays a spread

$$\Delta\Omega \approx \sqrt{\sum\nolimits_i \left(\frac{\partial \Omega}{\partial \gamma_i} \cdot \Delta\gamma_i\right)^2} \tag{7}$$

as approximated by Gaussian error propagation (for small $\{\Delta\gamma_i\}$ and mutually independent $\{\gamma_i\}$). Operationally robust valving can thus only be assured if the spin rate ω is moved across the frequency band $\Omega \pm M \cdot \Delta\Omega$; the factor M determines the level of functional reliability P_M evaluated by $1 - \mathrm{erf}\,[M/\sqrt{2}]$ with the error function "erf"; so, for $M \in \{1,2,3,4, \dots\}$, valving reliability can be gauged at $P_M \approx \{68\%, 95\%, 99.7\%, 99.99\%, \dots\}$.

Laboratory Unit Operations

Common bioanalytical assay panels are implemented on most LoaD platforms by batch-wise "stop-and-go" processing. To this end, the bioanalytical protocols are dissected into laboratory unit operations (LUOs), each of them controlled by normally closed valve. Centrifugally implemented LUOs have been covered extensively in the literature, e.g., for metering / aliquoting [45-47], mixing [48-51], incubation, purification / concentration / extraction [35, 52], homogenisation [53, 54], particle filtering [55-59] and droplet generation [60-62].

From a fluidic point of view, each LUO is typically executed by the interplay of a spin protocol $\omega(t)$, possibly featuring steeper ramps $d\omega/dt$, with a specifically shaped chamber upstream of the valve. For the important LUO of plasma separation, a minimum field strength

$$f_\omega = \Delta\varrho \cdot \mathcal{R} \cdot \omega^2 \tag{8}$$

Preprints (www.preprints.org) | NOT PEER-REVIEWED | Posted: 13 May 2021 doi:10.20944/preprints202105.0282.v1

Is required acting on a particle (or volume element) of differential density $\Delta\varrho$ with respect to its suspending (liquid) medium at radial position $\mathcal{R}$. For allowing proper operation of the rotationally actuated (high-pass) valve at its outlet, $\omega(t) < \Omega$ must be observed.

Design Optimization

Multiplexing

The sample-to-answer automation and parallelization of bioanalytical protocols representing comprehensively parallelized, multi-analyte assay panels including elements like calibrants, redundancies and dilution series is enabled by fluidic larger-scale integration (LSI) in the backend [42]. Towards high packing density, each valve design Γ_i hence needs to curtail their footprint in the radial, aerial and frequency domain, while concurrently meeting additional requirements, such as allowing a certain field strength f_ω (8) to assure proper execution of its upstream LUO.

A typical task in fluidic LSI of LoaD systems is thus to tailor a valve structure Γ_i for fitting into unoccupied radial and azimuthal intervals at the radial location R while squeezing its band $\Omega_i \pm M \cdot \Delta\Omega_i$ associated with tolerances $\{\gamma_i\}$ into an allowed ω-corridor.

Parameter Space

The radial space $R_{\min} < r < R_{\max}$ practically available for placing the valving structures $\{\Gamma_i\}$ is confined between the minimum and maximum structurable and bondable positions $R_{\min}$ and $R_{\max}$ inside the surface of the disc radius. There might be further boundary conditions for the parameters γ_i and resulting geometrical features of Γ_i, e.g., on minimum and maximum dimensions, adequate wall thicknesses, bending radii, draft angles, contact surface, aspect ratios related to manufacturing and assembly.

The upper boundary of the frequency envelope within which LoaD can be operated is limited to $\omega_{\max}$ by factors like the maximum torque of the spindle motor, the aerodynamic drag of the LoaD cartridge and its rotor, the pressure tightness of the chip assembly and safety concerns. There may also be a lower limit $\omega_{\min}$, e.g., required to broadly suppress uncontrolled capillary flow by a dominant centrifugal pressure $p_\omega \propto \omega^2$ (1), which is roughly achieved in the range $\omega > 10$ Hz, see back of the envelope calculation in the context of p_Θ (3). Thus, there is only a finite ω-space available for the bands $\{\Omega_i \pm M \cdot \Delta\Omega_i\}$ associated with the (joint) critical spin rate $\{\Omega_i\}$ (5,6) of each independently operated bunch of valves.

While the use of disc space is mainly linked to the geometry Γ and its radial position R, the tolerances $\{\Delta\gamma_j\}$ in experimental parameters $\{\gamma_j\}$ sensitively affect the band width $2 \cdot M \cdot \Delta\Omega$ (7). Guidelines for the systematic minimization of the standard deviation $\Delta\Omega_i = \Delta\Omega_i(\{\gamma_j\})$ will thus play a pivotal role in the subsequently discussed design optimization.

Performance Metrics / Criteria

This section presents a suite of metrics $\{\mathcal{M}_k\}$ to be minimized in order to achieve specific design goals towards fluidic LSI. Each of these metrics $\{\mathcal{M}_k\}$ depends on several (experimental) parameters $\{\gamma_j\}$ and their standard deviations $\{\Delta\gamma_i\}$, i.e., $\mathcal{M}_k = \mathcal{M}_k(\{\gamma_j, \Delta\gamma_i\})$. By convention, these metrics $\{\mathcal{M}_k\}$ are defined here to approach zero towards the targetted design goal, and unity for its largest (practical) value, i.e., $0 \leq \mathcal{M}_k \leq 1$. Design optimization of a given structure Γ_i according to a metric $\mathcal{M}_k$ thus comes down to their minimization in multidimensional space constituted by the variables $\{\gamma_j, \Delta\gamma_i\}$.

Geometries Γ_i derived in isolation, i.e., from reducing a single metric $\mathcal{M}_k$, tend to have very questionable benefit towards LSI. For example, a minimum spatial footprint may be associated with a

Preprints (www.preprints.org) | NOT PEER-REVIEWED | Posted: 13 May 2021 doi:10.20944/preprints202105.0282.v1

band width of the same magnitude as the entire ω-corridor, thus detrimentally undermining multiplexing. In the examples presented, we therefore relate most metrics $\mathcal{M}_k$ to the standard deviation $\Delta\Omega$.

In theory, the entire (available) multiparameter space $\{\gamma_j, \Delta\gamma_i\}$ must probed to spot the absolute minimum of $\mathcal{M}_k$, which would commonly require enormous computational power. Efficient numerical algorithms rather seek local minima by following the steepest local (downward) slope. By choosing, either statistically, or via a clever educated guess, a favorable starting point, at least a sufficiently small value for $\mathcal{M}_k$ may still be identified. In practice, convergence of the numerical methods within reasonable boundaries in multidimensional parameter space $\{\gamma_j, \Delta\gamma_i\}$ involves iterative "hinting" promising initial locations to the program. Therefore, the subsequent structures Γ might not represent absolute minima of the target metric(s) $\mathcal{M}_k$, but rather disclose value for deriving instructive design guidelines.

Component- and device-level optimization of a valving structure Γ usually needs to consolidate an array of possible contradictory demands, e.g., on minimum field strength f_ω (8), radially outbound staggering of LUO-valve for serial processing, non-overlapping stacking bands $\{\Omega_i \pm M \cdot \Delta\Omega_i\}$ (7), and surface area required for holding volumes of compression chambers V_C, liquid samples and reagents $\{U_{0,i}\}$ required by the assay protocol. We thus discuss the concept of multi-parameter optimization in the final subsection.

Band Width

The operational robustness of rotationally controlled valves correlates with their standard deviation $\Delta\Omega$ (7). This spread varies with parameters like R, Γ, U_0 and p_0, and their tolerances $\{\Delta\gamma_i\}$ mainly owing to precision of manufacturing, assembly, liquid metering and the ambient pressure p_0. For a CP-DF siphon valve with default geometry Γ (Figure 1), the dependency of $\Delta\Omega$ on the compression volume $V_{\mathrm{C},0}$ with common geometrical manufacturing tolerances $\Delta\gamma_i$ (Appendix), and the precision of the loaded liquid volume ΔU_0 is displayed in Figure 2. Accordingly, if disc space and radial ordering allows, it is favorable to enlarge the (primary) volume $V_{\mathrm{C},0}$ compression chamber until the curve saturates (Figure 2a), and to move Γ to outer radial positions R (Figure 2b).

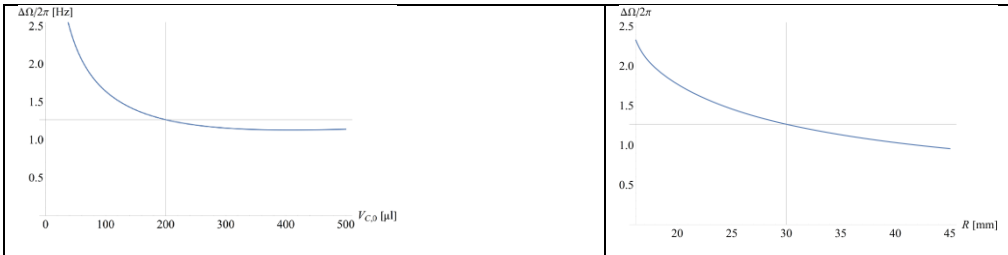

(a) $\Delta\Omega/2\pi$ vs. volume of the main compression chamber $V_{\mathrm{C},0}$ of Γ with $R = 3$ cm.

(b) $\Delta\Omega/2\pi$ vs. the radial position R of Γ.

Figure 2 Standard deviation $\Delta\Omega/2\pi$ for CP-DF siphon valves (with default parameters, see Appendix) as a function of (a) the volume of the main compression chamber $V_{\mathrm{C},0}$, and (b) the radial position R for typical dimensional (manufacturing) tolerances.

As already pointed out, the band width $\Delta\Omega$ (7) assumes a pivotal role in directing the layout of centrifugal microfluidic LoaD systems. Common optimization tasks of valving structures Γ in multiplexed liquid handling scenarios are thus often intertwined with keeping the spread $\Delta\Omega$ of each valving step at bay. We introduce the normalized metric

$$\overline{\Delta\Omega} = \frac{\Delta\Omega}{\omega_{\max} - \omega_{\min}} \tag{9}$$

Preprints (www.preprints.org) | NOT PEER-REVIEWED | Posted: 13 May 2021 doi:10.20944/preprints202105.0282.v1

for its computational optimization.

Refined Geometry

In order to improve options for minimization $\Delta\Omega$ (7), or $\overline{\Delta\Omega}$ (9), we have advanced the design of the valve Γ by compartmentalizing the most critical segments (Figure 1d). Figure 3 discloses that the increased dimensions of the parameters space γ_i permit reducing the spread $\Delta\Omega/2\pi$ from 0.95 Hz to 0.86 Hz for the same $R = 3$ cm and release rate $\Omega/2\pi \approx 25$ Hz. For $M = 4$, this would correspond to a lowering of the band width $M \cdot \Delta\Omega/\pi$ from 5.70 Hz to 5.16 Hz. Even more reduction in $\Delta\Omega$ is expected for more challenging cases, e.g., for enabling elevated retention rates Ω (5,6).

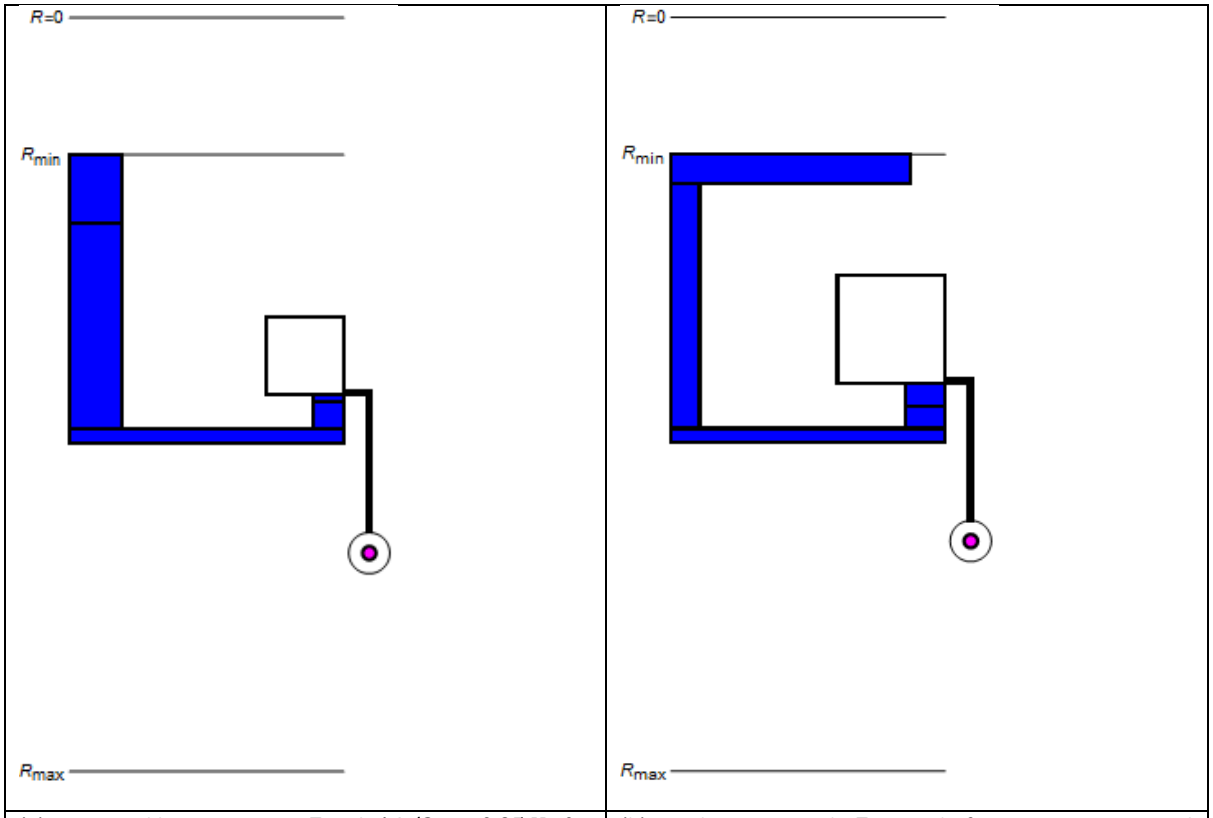

(a) Optimized base geometry Γ with $\Delta\Omega/2\pi \approx 0.95$ Hz for typical tolerances.

(b) Multi-segmented Γ tuned for minimum spread $\Delta\Omega/2\pi \approx 0.85$ Hz.

Figure 3 Comparison between structures Γ in their (a) basic and (b) multi-segmented versions for typical tolerances $\{\Delta\gamma_i\}$ at identical radial position $R = 3$ cm and release rate $\Omega/2\pi = 25$ Hz after optimization of $\Delta\Omega$. Most notably, Γ in (b) displays a wider inner radial section of the reservoir and overall increased width of the inbound segment to "pin" the menisci at r_0 and $r = R_{\mathrm{crest}}$, and thus $\bar{r}\Delta r$, to counter variation in Ω (5,6) via $\bar{r}\Delta r$.

Retention Rate and Field Strength

Liquids loaded to high-pass valves (Figure 1) are held back for $\omega < \Omega \propto (\bar{r}\Delta r)^{-1/2}$ (5); considering that $\bar{r}$ closely relates to the distance from the centre of rotation R, the structure Γ may be configured for a given liquid volume U_0 (exceed the dead volume of Γ outside R_{crest}) to minimize the difference in liquid levels Δr between the inlet reservoir and the radially inbound section; at least mathematically, Ω (5) can be tuned to any arbitrarily high value. For the specific case of CP-DF siphon valves (Figure 1) primarily investigated here, the scaling $\Omega \propto (V_{\mathrm{C}}/V - 1)^{1/2}$ (6) reveals that Ω also increases with the compression ratio V_{C}/V between the initial and the final volumes V_{C} and V of the enclosed gas pocket, respectively.

Preprints (www.preprints.org) | NOT PEER-REVIEWED | Posted: 13 May 2021 doi:10.20944/preprints202105.0282.v1

However, especially minimizing the compression volume V_C, or the liquid level difference Δr (not shown), entails a sharply increasing $\Delta\Omega$ (Figure 2a). Hence, in most cases, maximizing the retention rate Ω (5) needs to be carried out while confining $\Delta\Omega$ (7) to reasonable territories in ω-space.

As a typical LUO requiring maximization of Ω while limiting $\Delta\Omega$ for compatibility with LSI, we look at centrifugal sedimentation which is governed by the field strength $f_\omega = \Delta\varrho \cdot \mathcal{R} \cdot \Omega^2$ (8) experienced by a particle of density differential $\Delta\varrho$ with respect to the suspending medium at the radial position $\mathcal{R}$ and retention rate Ω. The metric

$$\bar{f}_\omega = \frac{\mathcal{R} \cdot \Omega^2}{R_{\max} \cdot \omega_{\max}^2} \tag{10}$$

may be used for optimizing the field strength f_ω on a disc. In many cases, $\mathcal{R} \approx R$.

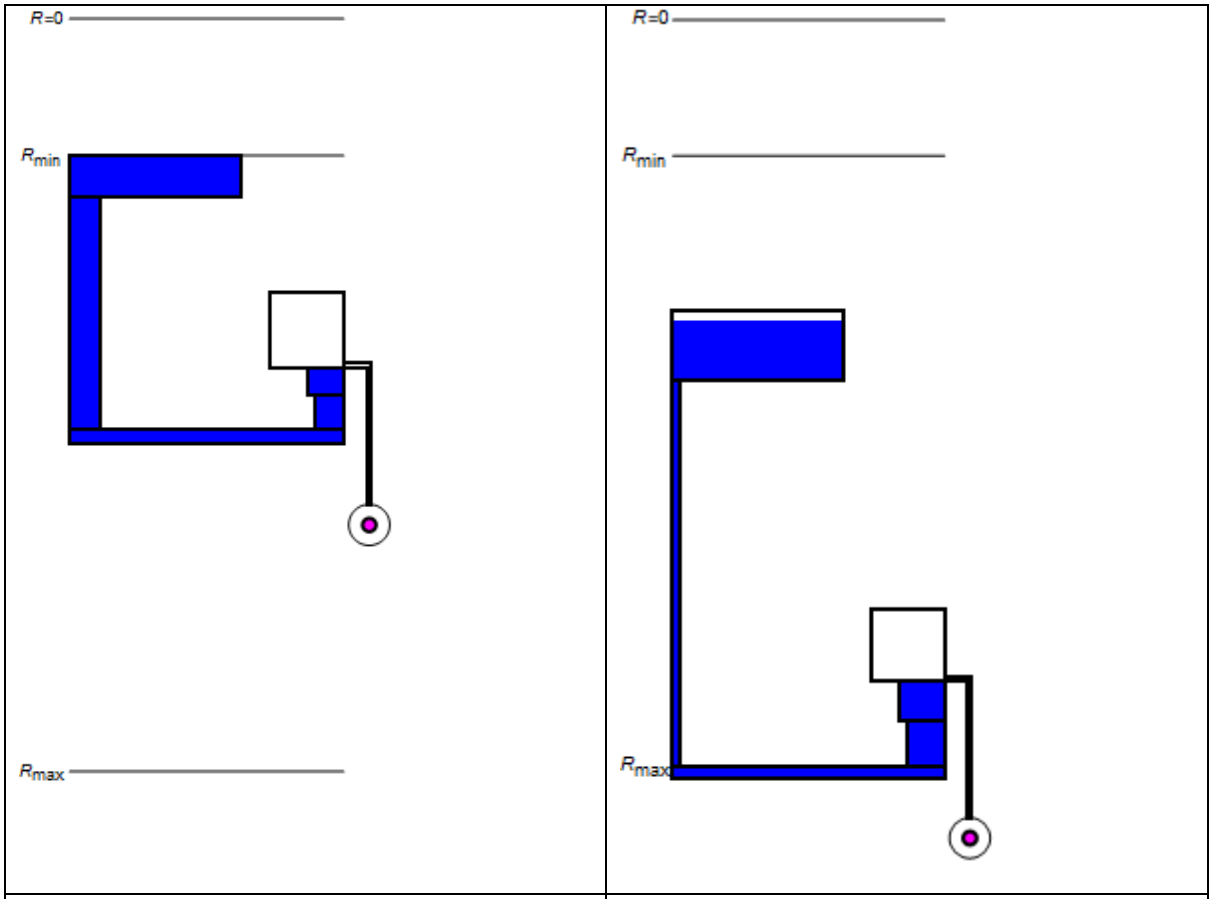

(a) Minimized $\Delta\Omega$ at $R = 3$ cm: $\Omega/2\pi \approx 45$ Hz and $\Delta\Omega/2\pi \approx 1.34$ Hz.

(b) Minimized $\Delta\Omega$ at $R = 5$ cm: $\Omega/2\pi \approx 31$ Hz, to establish the same field strength f_ω as at $R = 3$ cm as in (a), and $\Delta\Omega/2\pi \approx 1.03$ Hz.

Figure 4 (a) Optimizing the band width at (a) $R = 3$ cm and $\Omega\ /2\pi = 40$ Hz with $\Delta\Omega\ /2\pi \approx$ and (b) at $R = 5$ cm by reducing Ω to establish the same field strength $f_\omega \propto R \cdot \Omega^2$ (8), with $\Delta\Omega\ /2\pi \approx 1.03$ Hz.

Figure 4 shows how the multi-segmented structure Γ (Figure 1d) can be adjusted to minimize $\Delta\Omega$ while providing the same field strength f_ω (8) at both representative radial locations $R = 3$ cm (a) and 5 cm (b). Such a design task may occur if the location of the particle sedimentation needs to be radially shifted, for instance, towards the center to occur at an earlier stage at a serial liquid handling sequence, or to be placed where space is more ample in the outer region of the disc.

Preprints (www.preprints.org) | NOT PEER-REVIEWED | Posted: 13 May 2021 doi:10.20944/preprints202105.0282.v1

Concurrent Valving

For their simultaneous rotational actuation, valves ideally share the same Ω to save precious ω-space. However, it may often be necessary to place their structures $\{\Gamma_i\}$ at the different radial position $\{R_i\}$. Figure 5 shows how Γ is altered at inner and (extreme) outer locations $R = 3$ cm (a) and 5.5 cm (b) to minimize $\Delta\Omega$ while maintaining the same $\Omega/2\pi = 25$ Hz.

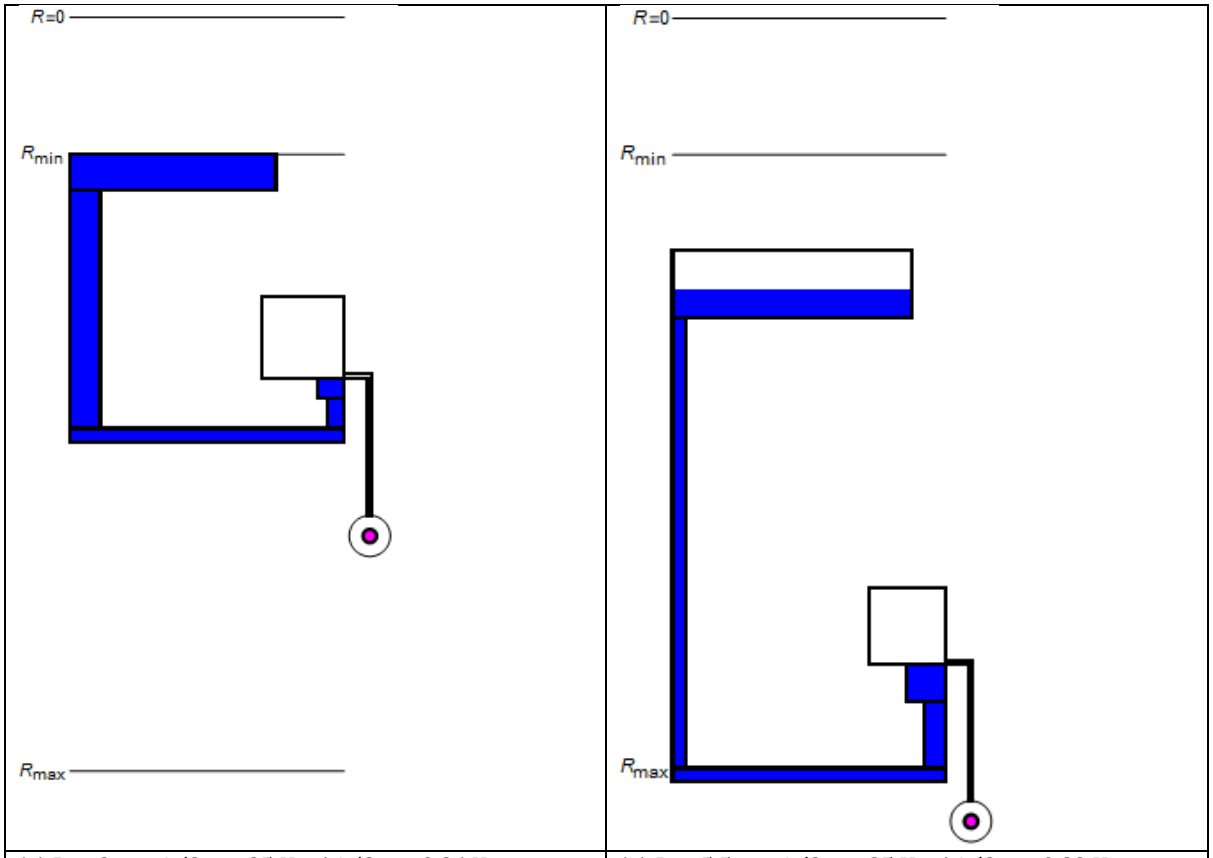

(a) $R = 3$ cm, $\Omega/2\pi \approx 25$ Hz: $\Delta\Omega/2\pi \approx 0.86$ Hz. (b) $R = 5.5$ cm, $\Omega/2\pi \approx 25$ Hz: $\Delta\Omega/2\pi \approx 0.83$ Hz.

Figure 5 Minimization of band width $\Delta\Omega$ for a set of CP-DF siphon valves Γ possessing equal retention rates $\Omega/2\pi = 25$ Hz which are placed the radial positions (a) $R = 3$ cm and (b) $R = 5.5$ cm.

Radial Space

Factoring in the limited spacing between $R_{\min}$ and $R_{\max}$, and the need for outbound staggering of serial LUOs, valving structures Γ should also be taxed for the radial interval

$$\bar{R} = \frac{R - r_0}{R_{\max} - R_{\min}} \tag{11}$$

they cover between their inner- and outermost confinements r_0 in the inlet and R (neglecting $d_{\text{iso}} \ll R$) of Γ, respectively (Figure 1a). Figure 6 illustrates structures Γ that have been optimized for consuming minimum radial interval $\bar{R}$ (11) at $R = 3$ cm (a) and 5 cm (b).

Preprints (www.preprints.org) | NOT PEER-REVIEWED | Posted: 13 May 2021 doi:10.20944/preprints202105.0282.v1

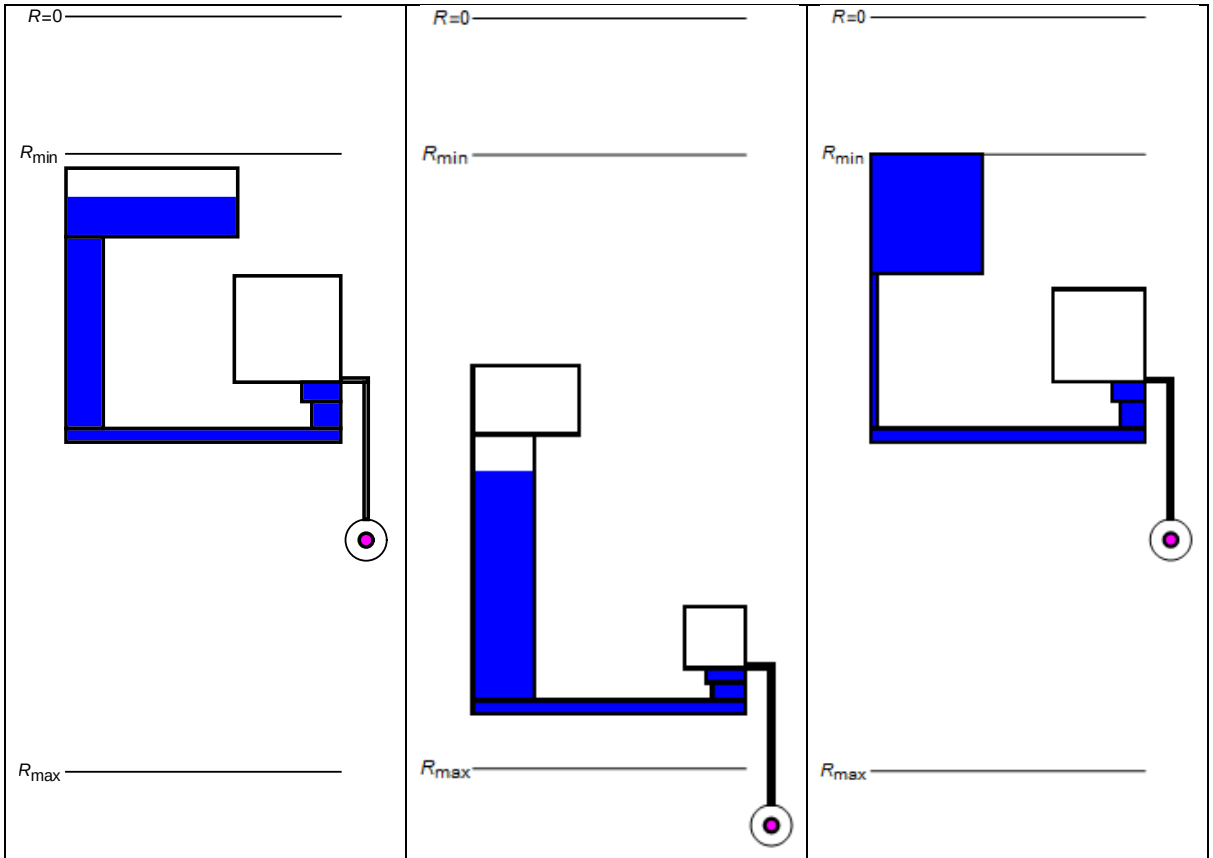

(a) Radial footprint $\overline{\Delta r}$ of Γ reduced to $1.8\ \mathrm{cm}$ at $R = 3\ \mathrm{cm}$ with $\Delta\Omega\ /2\pi \approx 0.87\ \mathrm{Hz}$.

(b) Radial footprint $\overline{\Delta r}$ of Γ reduced to $1.8\ \mathrm{cm}$ at $R = 5\ \mathrm{cm}$ with $\Delta\Omega\ /2\pi \approx 0.95\ \mathrm{Hz}$.

(c) Minimization of areal footprint $\bar{A}$ (excluding compression chamber) with of $\Delta\Omega/2\pi \approx 0.86\ \mathrm{Hz}$.

Figure 6 Geometrical optimization of Γ towards minimum band width $\Delta\Omega$ at a given $\Omega/2\pi = 25\ \mathrm{Hz}$ towards minimum radial extension $\overline{\Delta R}$ (11) at the radial positions (a) $R = 3\ \mathrm{cm}$, (b) $R = 5\ \mathrm{cm}$, and towards (c) smallest spatial footprint $\bar{A}$ (13) at $\Omega/2\pi \approx 25\ \mathrm{Hz}$. (c)

Furthermore, LUOs occurring early in the protocol, e.g., particle sedimentation or initial metering of loaded liquids, may need to be placed more centrally in order to allow radially outbound staggering of subsequent operations within the interval $R_{\min} \leq r_0 < R_{\mathrm{crest}} \leq R_{\max}$. The metric

$$\check{R} = 1 - \frac{R}{R_{\max}} \tag{12}$$

might then be minimized to configure geometries Γ for placement near the centre of rotation at $r = 0$. However, especially for LUOs requiring high field strength f_ω (8), this comes at the expense of larger band width $\Delta\Omega$ (see also Figure 2b).

Spatial Footprint

Owing to the rotational symmetry of LoaD systems, overall disc space is scarce. We define the metric

$$\bar{A} = \frac{A_\Gamma}{\pi \cdot (R_{\max}^2 - R_{\min}^2)} \tag{13}$$

which relates the total surface area A_Γ claimed by Γ, possibly excluding the flexibly placeable compression chamber, to the structurable annular region extending between $R_{\min}$ and $R_{\max}$. Figure 6c presents a structure Γ which has been configured for low $\bar{A}$ (13) for $\Omega/2\pi = 25\ \mathrm{Hz}$ while, at the same time, maintain low band width $\Delta\Omega$ (7). As the manufacturing tolerances only account for a small fraction of the absolute dimensions of Γ, they do not substantially alter the absolute and relative

Preprints (www.preprints.org) | NOT PEER-REVIEWED | Posted: 13 May 2021 doi:10.20944/preprints202105.0282.v1

spatial footprints A_Γ and $\bar{A}$ (13), respectively. To reflect that central space is most precious, a combination of the metrics $\bar{R}$ (11), $\check{R}$ (12) and $\bar{A}$ (13) may be employed for optimization.

Definition of Liquid Volumes

In a centrifugally automated bioanalytical protocols, the precision $\Delta U_{0,i}$ of loaded liquid volumes $U_{0,i}$ by structures Γ_i directly enter mixing ratios of sample and reagents, and thus assay quantitation, as well as valving performance in terms critical spin rates Ω (5), mostly through the radial product $\bar{r}\Delta r$ reflecting the spatial distribution $\Lambda = \Lambda(U_0)$. Uncertainties ΔU_0 in U_0 occur during introduction the liquid into Γ through pipetting, and subsequent serial transfer through LUOs and their valves before arriving in a final, end-point detection chamber.

Figure 7a reveals the significant growth $\Delta\Omega$ with the spread ΔU_0 (with otherwise default tolerances $\{\Delta\gamma_i\}$, see Appendix); the structure Γ in Figure 7b has been optimized to keep the standard deviation $\Delta\Omega$ at bay for (rather large) $\Delta U_0 = 10$ µl.

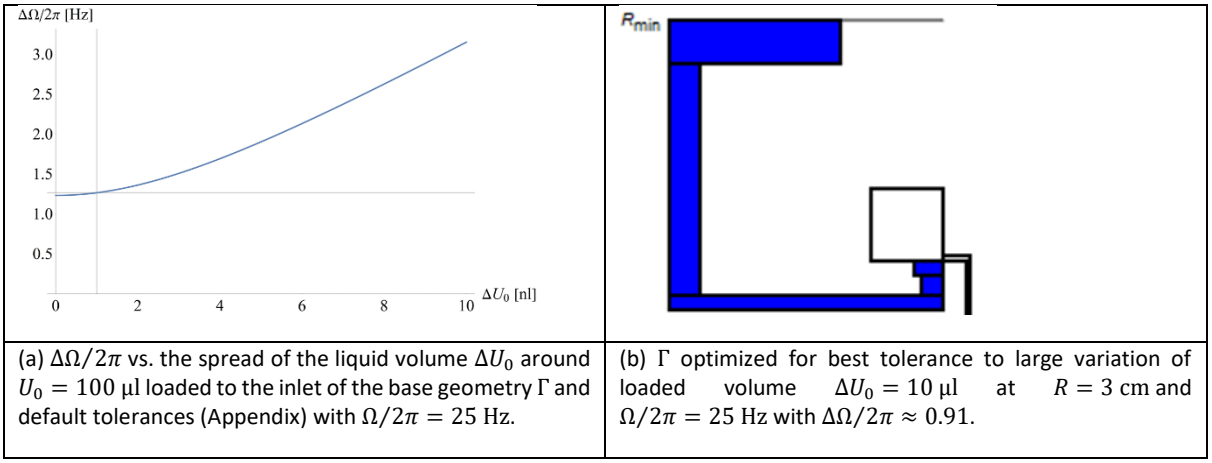

(a) $\Delta\Omega/2\pi$ vs. the spread of the liquid volume ΔU_0 around $U_0 = 100$ µl loaded to the inlet of the base geometry Γ and default tolerances (Appendix) with $\Omega/2\pi = 25$ Hz.

(b) Γ optimized for best tolerance to large variation of loaded volume $\Delta U_0 = 10$ µl at $R = 3$ cm and $\Omega/2\pi = 25$ Hz with $\Delta\Omega/2\pi \approx 0.91$.

Figure 7 (a) Band width $\Delta\Omega$ as a function of the precision of the loaded volume ΔU_0 with default other values $\Delta\gamma_i$ (Appendix). (b) Structure Γ (excerpt) optimized for minimum standard deviation $\Delta\Omega$ caused by the spread ΔU_0.

On the outlet side, valves retain a certain fraction of the introduced liquid volume U_0. While reproducible losses U_{loss} may readily be compensated via the layout according to (5, 6), they tend to increase space requirements; their impact can be mitigated through minimizing the metric

$$\bar{U}_{\text{loss}} = \frac{U_{\text{loss}}}{U_0} \approx \frac{d_0 \cdot w_0 \cdot (R - r_0) + U_{\text{iso}} + d \cdot w \cdot Z}{U_0} \tag{14}$$

which assumes that the entire liquid filling Γ below its crest point R_{crest} will not be transferred open actuation in a purely overflow driven valve (see Figure 1 for parameter definitions).

Assuming that deviations from this model mainly result from pulley effects of the liquid plug of volume $d \cdot w \cdot Z$ residing in the inbound segment (Figure 1), the metric

$$\overline{\Delta U}_{\text{loss}} = \frac{\Delta U_{\text{loss}}}{U_{\text{loss}}} \approx \frac{d \cdot w \cdot Z}{d_0 \cdot w_0 \cdot (R - r_0) + U_{\text{iso}} + d \cdot w \cdot Z} \tag{15}$$

accounts for its statistical variations ΔU_{loss} with respect to the total residual volume U_{loss}. The value of $\overline{\Delta U}_{\text{loss}}$ (15) should ideally vanish to minimize the band width $\Delta\Omega$ (7) and the related bioanalytical precision, which is the case for merely overflow driven liquid transfer to the outer DF chamber.

Ambient Pressure

In the context of the definition of p_ω (1), it was already calculated that the rotationally induced pressure head only amounts to a smaller portion of the actual ambient pressure p_0. Therefore, the retention rate $\Omega \propto \sqrt{p_0}$ (6) of centrifugo-pneumatic valves reacts rather sensitively to (typically slow)

Preprints (www.preprints.org) | NOT PEER-REVIEWED | Posted: 13 May 2021 doi:10.20944/preprints202105.0282.v1

changes of the atmospheric pressure p_0, e.g., caused by local altitude or weather. Figure 8a displays the shift of the retention rate Ω over a range of typical, weather-related variations in p_0' of about 4%. Even larger changes are impacted with local altitude, roughly 10% per $1000\ \mathrm{m}$. It therefore makes sense to link a pressure sensor to a LoaD instrument to adjust the spin protocol $\omega(t)$ to local ambient pressure p_0, which tend to stay fairly constant over the course of an assay.

Strictly speaking, formula (6) assumes that the ambient pressure p_0 is equal to the pressure of the air entrapped in the compression chamber at the point of complete filling of the isoradial segment (Figure 1a). However, hydrodynamic effects might lead to deviations which we consider by extending (6)

$$\Omega = \sqrt{\frac{(1+\chi)\cdot p_0 \cdot (V_C/V - 1)}{\varrho \cdot \bar{r}\Delta r}} \tag{16}$$

with the unitless factor $\chi = p_0'/p_0 - 1$ reflecting the fractional divergence of the actual pressure p_0' in the compression chamber at the point of pneumatic cut-off from the ambient pressure at p_0 [39]. Figure 8b shows that deviations $|\chi| > 0$, which are hard to measure in practice, should be kept in the permille range, or at least be reproducible, i.e., $\Delta\chi \approx 0$, to allow compensation by modulating $\omega(t)$, to avoid having a massive impact on the band width $\Delta\Omega$ (7).

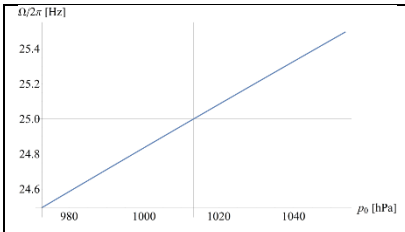

(a) Variation of the retention rate Ω with the actual ambient p_0 near $p_{\mathrm{std}} = 1013.25$ hPa.

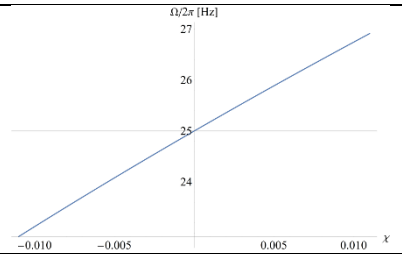

(b) Variation of the retention rate Ω with $\chi = p_0'/p_0 - 1$ for changes up to about $\pm 1\%$.

Figure 8 Variation of retention rate Ω vs (a) actual atmospheric pressure p_0 and (b) with the fractional deviation $\chi = p_0'/p_0 - 1$ of the pressure of the enclosed gas pocket p_0' from p_0 at the point of isolation from atmosphere. Note that variations in χ of more than a few permille have a considerable impact on Ω (5,6,16).

Manufacturing – Process Limitations and Costs

From a mere fluidic and mathematical point of view, elementary spatial needs may be captured rather well by $\bar{R}$ (11), $\check{R}$ (12) and $\bar{A}$ (13). Yet, in practice, the degree of freedom for designing structures Γ, and their packing density empowering fluidic multiplexing, is further influenced by materials and their processing technologies along prototyping, pilot series and (commercial) mass fabrication, the latter typically based on tool-based polymer replication and pick-and-place assembly schemes [43].

This repertoire of fabrication techniques commonly involves different dimensional tolerances, and often imposes considerably differing types and magnitudes of design restrictions, e.g., on minimum feature sizes, aspect ratios, wall thicknesses, draft angles, the homogeneity of packing density and the distribution of hydrodynamic resistances (for mold flow and demolding), curvature of concave or convex edges on tools and their replicates, and sufficient interstitial and peripheral surface area for pressure-proof bonding.

Furthermore, not all area unoccupied by Γ may be available for other structures, e.g., as it may be too small or occluded in the centre of a neighbouring Γ. While these restrictions are hard to exactly quantify, they might be, more or less, captured by a reserving a “fringe” corresponding the minimum wall thickness or bonding surface around the outer contours of Γ.

Thus, in addition to the fluidic aspects mostly addressed in this work, future endeavors should be directed towards factoring in the design optimization towards criteria associated with manufacture

Preprints (www.preprints.org) | NOT PEER-REVIEWED | Posted: 13 May 2021 doi:10.20944/preprints202105.0282.v1

and assembly, and their effect on technological complexity and related cost of development and production [63].

Multi-Parameter Optimization

Given the complexity of these often somewhat conflicting design targets, a multi-parameter optimization usually needs to be implemented computationally along the combined metric

$$\mathcal{M} = \sum_k c_k \cdot \mathcal{M}_k \tag{17}$$

to be minimized. Each constituent metric $\mathcal{M}_k$ (17) is weighted by a numerical coefficient c_k, optionally imposing normalization $\sum_k c_k = 1$. For instance, amongst the numerous possible scenarios, a valving structure Γ may need to be geared to facilitate a certain (minimum) field strength f_ω (8) while its band $\Omega \pm M \cdot \Delta\Omega$ (5) and radial extension $\bar{R}$ (11) need to fit into their accessible corridors in real and frequency space, respectively. Accordingly, the aggregate metric

$$\mathcal{M} = c_{f_\omega} \cdot \overline{f_\omega} + c_R \cdot \bar{R} + c_{\Delta\Omega} \cdot \overline{\Delta\Omega} \tag{18}$$

ought to be minimized within the available radial and frequency spaces, and, in the simplest case, with equal coefficients $c_{f_\omega} = c_R = c_{\Delta\Omega} = 1/3$.

General Design Guidelines

Fitting a structure Γ into a given, still available "slot" in both, real and frequency space thus represents a primary design goal directing the layout of multiplexed LoaD systems. In absence of a universal design recipe in view of the plethora of possible application cases, a few important, partially counteracting trends can still be pointed out.

The retention rate Ω (6) of a CP-DF siphon valve is chiefly affiliated with its radial position R and geometry Γ, the liquid volume U_0 of density ϱ, and the ambient pressure p_0. Large Ω are achieved towards high ratios V_C/V between the initial and final volumes of the compression chamber, and small radial product $\bar{r}\Delta r$. Consequently, high field strengths $f_\omega \propto R \cdot \Omega^2$ (8) at narrow $\Delta\Omega$ (Figure 2b) are best established at outer radial positions R.

The quotient V_C/V is directly related to the statically defined structure Γ. Moreover, the product $\bar{r}\Delta r$ immediately derives from the meniscus positions r_0 and r in the inlet reservoir and inbound segment, respectively. In the general case, these levels confining the liquid distribution Λ emerge in response to the centrifugal, pneumatic and ambient pressures p_ω (1), p_V (2), and p_0. Yet, for $\omega = \Omega$, $r = R_{\mathrm{crest}} = R - Z$ (Figure 1a), so r_0 becomes a function of Γ and U_0, and overall, $\Omega = \Omega(R, \Gamma, U_0, \varrho, p_0)$. The free experimental parameters to set Ω are typically R, Γ and U_0, while ϱ is prescribed by the assay and p_0 by the local altitude, temperature and weather.

Furthermore, any tolerances $\Delta R, \Delta\Gamma, \Delta U_0, \Delta\varrho$ and Δp_0 in their corresponding input parameters R, Γ, U_0, ϱ and p_0, and a possibly $\chi \neq 0$ (16) echoing the filling dynamics, lead to a spread $\Delta\Omega$ in the retention rate Ω. In most application setups, the actual ambient pressure $p_0 \neq p_{\mathrm{std}}$ may be measured and remains reasonably constant over the course of a bioassay. Hence, statistical fluctuations Δp_0 can be neglected, i.e., $\Delta p_0/p_0 \ll 1$, which can also be assumed for the density, i.e., $\Delta\varrho/\varrho \ll 1$. Irreproducible filling procedures (Figure 1) may lead to statistical deviations $\Delta\chi \approx 0$, which may have a significant impact on Ω (16) if exceeding the permille range (Figure 8b). Measures like slow, quasi-static loading of the liquid, an optimized shape of the inlet reservoir and a high hydrodynamic resistance of the isoradial channel are thus advisable.

With these considerations taken into account, the standard deviation $\Delta\Omega$ mainly represents a function of the pipetting precision ΔU_0 and the dimensional manufacturing tolerances $\Delta\Gamma$; importantly, these

Preprints (www.preprints.org) | NOT PEER-REVIEWED | Posted: 13 May 2021 doi:10.20944/preprints202105.0282.v1

variations are either well known from manuals or literature, or can rather easily be determined for a particular material and its processing technique from comparatively simple, general-purpose test structures to generally inform $\Delta\Omega$ for a wide range of designs Γ. This way, the (costly) manufacture of a large, statistically sufficient number of LoaD devices can be bypassed.

Restricting the band width $\Delta\Omega$ turns out to be particularly challenging towards large Ω. Figure 2 advises that $\Delta\Omega$ reduces towards increasing compression volumes V_C and outer radial positions R. This is reasoned by the decreasing (relative) influence of manufacturing tolerances $\{\Delta\gamma_i\}$ defined on an absolute scale towards growing structural dimensions of Γ. Furthermore, any tolerances $\Delta\Gamma$ or ΔU_0 intimately affect the magnitude of the radial product $\bar{r}\Delta r$. To stabilize both, $\bar{r}$ and Δr, the minimization of the band width $\Delta\Omega$ thus typically involves widening of the radially inner segments near their meniscus positions r_0 and R_{crest} assumed in the vicinity of the retention rate $\omega = \Omega$.

The results presented here for the optimized structures Γ show that the typical standard deviation of Ω ranges in the order of $\Delta\Omega/2\pi \approx 1$ Hz. To assess the impact on robust fluidic multiplexing, we consider the rotationally actuated serial release of N simultaneously loaded liquids, with each valve operating at a component-level reliability $P_M = 99.99\%$ for $M = 4$; for this case, the width of the band $\Omega \pm M \cdot \Delta\Omega$ calculates to $2 \cdot M \cdot \Delta\Omega \approx 8$ Hz. Consequently, a frequency envelope spanning over 40 Hz between $\Omega_{\mathrm{min}}/2\pi = 15$ Hz and $\Omega_{\mathrm{max}}/2\pi = 55$ Hz could, in theory, assure a high system-level robustness of $P_{M=4}^{N} \approx 99.96\%$ for $N = 5$ independent, rotationally controllable sets of (high-pass) valves.

However, this envelope is often "squeezed" into upper regions of the frequency space, i.e., reducing the frequency envelope $\Omega'_{\mathrm{min}} \gg \Omega_{\mathrm{min}}$. The new, higher boundary Ω'_{min} may be attributed to an LUO occurring early in the liquid handling protocol of an assay, such as plasma separation, which would require an inner position R of Γ, and thus a substantial spin rate $\Omega \gg \Omega_{\mathrm{min}}$, to provide a sufficient field strength f_ω (8) for guaranteeing efficient sedimentation. All simultaneously loaded, and later opened high-pass valves would, accordingly, have accommodate their bands in this much narrower frequency corridor.

Summary and Outlook

Large-scale integration (LSI) of fluidic networks constitutes a key prerequisite for comprehensive sample-to-answer automation of parallelized, multi-step / multi-reagent bioassay protocols suitable for application at the Point-of-Care. A digital twin concept for rotationally actuated flow control by centrifugo-pneumatic dissolvable-film (CP-DF) siphon valves on "Lab-on-a-Disc" systems operating in batch-mode was elaborated; to accomplish high functional packing density without sacrificing commercially critical operational robustness, it was shown that, in addition spatial footprint and radial placement, mainly the minimization of the standard deviation $\Delta\Omega$ arising from the limited precision of experimental input parameters assumes a crucial role.

Strategies were outlined to computationally optimize a suite of performance metrics of exemplary, highly configurable CP-DF siphon valves. The model-based approach offers a viable alternative to lengthy and expensive manufacture and experimental characterization at system level, which requires device numbers and testing facilities that are mostly unavailable at development stage and along scale-up using different manufacturing techniques.

It is to mention that, alternatively to fluidic LSI, multiplexed detection has also been achieved through other schemes such as bead-based or label-based methods, sometimes in combination with off-chip or fluidic sample preconditioning. The analysis of its pros and cons falls beyond the scope of this article. Generally speaking, such substitutional methods require common assay chemistries for all analytes,

Preprints (www.preprints.org) | NOT PEER-REVIEWED | Posted: 13 May 2021 doi:10.20944/preprints202105.0282.v1

and rather complex optical encoding or multi-wavelength detection; these enhanced technical demands need to comply with the cost base and ruggedness of the instrument for its deployment outside professional environments, and for markedly lower throughputs, e.g., in patient self-testing at home.

Future work should include more complex geometries, and flexible elements in the fluidic modelling, e.g., reflecting the bending of lids, compression and friction of trapped gas bubbles, and hydrodynamic effects, thus sophisticating design rules with even higher predictability of performance and reliability. The modelling should also include other, especially rotationally actuated valving and flow control techniques. To create more disc space, options of multilayer stacking may be explored.

In addition, simulation of fabrication processes and assay kinetics would clearly augment the digital twin approach. Eventually, professional layout software may be provided, which would, for instance, enable foundry services as a landmark of mature supply chains. Regarding the bigger picture, the publication of the digital twin sets the stage for open platform models that have been discussed in the context of crowdsourcing through, e.g., blockchain-backed, participatory research models [64-67].

Appendix: Default Valve Geometry

The structure Γ, their radial positions R and loaded by liquid volumes U_0 can be varied across a multi-dimensional parameter space, e.g., to tune retention rates Ω, or other key performance indicators. Table A1 provides of overview or generic values for the parameters displayed in Figure 1 which can be used to initiate optimization.

$R = 3$ cm	$R_{\mathrm{min}} = 1.5$ cm	$R_{\mathrm{max}} = 5.5$ cm	$R_{\mathrm{DF}} = 3.15$ cm $> R$
$A_0 = d_0 \cdot w_0$	$d_0 = 1$ mm	$w_0 = 5$ mm	
$U_0 = 100$ µl $< A_0 \cdot (R - R_{\mathrm{min}})$			
$U_{\mathrm{iso}} = d_0 \cdot h \cdot L \ll U_0$	$d_{\mathrm{iso}} = 1$ mm	$h_{\mathrm{iso}} = 1$ mm	$L_{\mathrm{iso}} = 15$ mm $> w_0 + w$
$U_Z = d \cdot w \cdot Z$	$d = 500$ µm	$w = 800$ µm $\ll w_0$	$Z = 10$ mm
$V_{\mathrm{C},0} = d_{\mathrm{C}} \cdot w_{\mathrm{C}} \cdot h_{\mathrm{C}} \gg U_Z$	$d_{\mathrm{C}} = 1$ mm	$w_{\mathrm{C}} = 20$ mm	$h_{\mathrm{C}} = 10$ mm
$V_{\mathrm{int}} = d_{\mathrm{int}} \cdot h_{\mathrm{int}} \cdot L_{\mathrm{int}} \ll V_{\mathrm{C}}$	$d_{\mathrm{int}} = 200$ µm	$h_{\mathrm{int}} = 300$ µm	$L_{\mathrm{int}} = 1$ cm $> 2w$
$V_{\mathrm{DF}} = 0.25\pi \cdot d_{\mathrm{DF}} \cdot D_{\mathrm{DF}}^2 \ll V_{\mathrm{C}}$	$d_{\mathrm{DF}} = 190$ µm	$D_{\mathrm{DF}} = 3$ mm	$\alpha = 0.45, \beta = 0.5$

Table A1 Default geometrical parameters and relationships of basic CP-DF siphon valves (Figure 1). The resulting critical spin rate $\Omega(R, \Gamma, U_0)/2\pi \approx 25$ Hz. Minimum lateral dimensions are given by the smallest practical diameter of milling tools (200 µm). As tools for injection molding are often adopted from optical data storage (e.g., CD, DVD, Blu-ray), a central, 1.5-cm diameter hole and a disc radius of 6 cm with thickness around 1.2 mm, fluidic structures Γ may need to stay within the radial interval between $R_{\mathrm{min}} = 1.5$ cm and $\mathrm{R}_{\mathrm{max}} = 5.5$ cm, and an upper limit for the depth of about 1 mm, as chosen for the main parts of geometries Γ. For large lateral extensions or small aspect ratios, sagging of the lid, which is often a rather flexible foil, may significantly change the nominal volume capacity, also in response to the pressure, and might even lead to sticking to the bottom of the cavity.

The default tolerances $\Delta\gamma_i$ in the chief input parameters γ_i are:

- Lateral structuring $\Delta w = \Delta h = 20$ µm
- Vertical structuring $\Delta d = 30$ µm
- Precision of liquid volume $\Delta U_0/U_0 = 1\%$
- Ambient pressure $\Delta p_0 = 40$ hPa

In the digital twin model, different standard deviations $\Delta\gamma_i$ may easily be plugged into the calculations.

References

1. Manz, A., N. Graber, and H.M. Widmer *Miniaturized total chemical analysis systems: A novel concept for chemical sensing*. Sensors and Actuators B: Chemical, 1990. **1**, 244-248 DOI: 10.1016/0925-4005(90)80209-I.

2. Reyes, D.R., D. Iossifidis, P.-A. Auroux, and A. Manz, *Micro Total Analysis Systems. 1. Introduction, Theory, and Technology.* Analytical Chemistry, 2002. **74**(12): p. 2623-2636.
3. Auroux, P.-A., D. Iossifidis, D.R. Reyes, and A. Manz, *Micro Total Analysis Systems. 2. Analytical Standard Operations and Applications.* Analytical Chemistry, 2002. **74**(12): p. 2637-2652.
4. Schembri, C.T., V. Ostoich, P.J. Lingane, T.L. Burd, and S.N. Buhl *Portable Simultaneous Multiple Analyte Whole-Blood Analyzer for Point-of-Care Testing*. Clinical Chemistry, 1992. **38**, 1665-1670 DOI: 10.1093/clinchem/38.9.1665.
5. Schembri, C.T., T.L. Burd, A.R. Kopfsill, L.R. Shea, and B. Braynin *Centrifugation and Capillarity Integrated into a Multiple Analyte Whole-Blood Analyzer*. Journal of Automatic Chemistry, 1995. **17**, 99-104 DOI: 10.1155/S1463924695000174.
6. *Abaxis*. Available on: https://www.abaxis.com.
7. Andersson, P., G. Jesson, G. Kylberg, G. Ekstrand, and G. Thorsen *Parallel nanoliter microfluidic analysis system*. Analytical Chemistry, 2007. **79**, 4022-4030 DOI: 10.1021/ac061692y.
8. Inganas, M., H. Derand, A. Eckersten, G. Ekstrand, A.K. Honerud, G. Jesson, G. Thorsen, T. Soderman, and P. Andersson *Integrated microfluidic compact disc device with potential use in both centralized and point-of-care laboratory settings*. Clinical Chemistry, 2005. **51**, 1985-7 DOI: 10.1373/clinchem.2005.053181.
9. *Gyros Protein Technologies*. Available on: https://www.gyrosproteintechnologies.com/.
10. Madou, M.J. and G.J. Kellogg *The LabCD (TM): A centrifuge-based microfluidic platform for diagnostics*. Systems and Technologies for Clinical Diagnostics and Drug Discovery, Proceedings Of, 1998. **3259**, 80-93 DOI: 10.1117/12.307314.
11. Shea, M. *ADMET Assays on Tecan's LabCD-ADMET System*. Journal of the Association for Laboratory Automation, 2003. **8**, 74-77 DOI: 10.1016/s1535-5535(04)00260-6.
12. Smith, S., D. Mager, A. Perebikovsky, E. Shamloo, D. Kinahan, R. Mishra, S.M.T. Delgado, H. Kido, S. Saha, J. Ducrée, M. Madou, K. Land, and J.G. Korvink *CD-Based Microfluidics for Primary Care in Extreme Point-of-Care Settings*. Micromachines, 2016. **7**, DOI: 10.3390/mi7020022.
13. Kong, L.X., A. Perebikovsky, J. Moebius, L. Kulinsky, and M. Madou *Lab-on-a-CD: A Fully Integrated Molecular Diagnostic System*. Journal of the Association for Laboratory Automation, 2016. **21**, 323-355 DOI: 10.1177/2211068215588456.
14. Maguire, I., R. O'Kennedy, J. Ducrée, and F. Regan *A review of centrifugal microfluidics in environmental monitoring*. Analytical Methods, 2018. **10**, 1497-1515 DOI: 10.1039/c8ay00361k.
15. Gorkin, R., J. Park, J. Siegrist, M. Amasia, B.S. Lee, J.M. Park, J. Kim, H. Kim, M. Madou, and Y.K. Cho *Centrifugal microfluidics for biomedical applications*. Lab on a Chip, 2010. **10**, 1758-1773 DOI: 10.1039/b924109d.
16. Burger, R., L. Amato, and A. Boisen *Detection methods for centrifugal microfluidic platforms*. Biosensors and Bioelectronics, 2016. **76**, 54-67 DOI: 10.1016/j.bios.2015.06.075.
17. Ducrée, J., S. Haeberle, S. Lutz, S. Pausch, F. von Stetten, and R. Zengerle *The centrifugal microfluidic Bio-Disk platform*. Journal of Micromechanics and Microengineering, 2007. **17**, S103-S115 DOI: 10.1088/0960-1317/17/7/S07.
18. Lutz, S., D. Mark, G. Roth, R. Zengerle, and F. von Stetten *Centrifugal Microfluidic Platforms for Molecular Diagnostics*. Clinical Chemistry and Laboratory Medicine, 2011. **49**, S608-S608.
19. Tang, M., G. Wang, S.-K. Kong, and H.-P. Ho *A Review of Biomedical Centrifugal Microfluidic Platforms*. Micromachines, 2016. **7**, DOI: 10.3390/mi7020026.
20. Duffy, D.C., H.L. Gillis, J. Lin, N.F. Sheppard, and G.J. Kellogg *Microfabricated Centrifugal Microfluidic Systems: Characterization and Multiple Enzymatic Assays*. Analytical Chemistry, 1999. **71**, 4669-4678 DOI: 10.1021/ac990682c.
21. Azimi-Boulali, J., M. Madadelahi, M.J. Madou, and S.O. Martinez-Chapa *Droplet and Particle Generation on Centrifugal Microfluidic Platforms: A Review*. Micromachines, 2020. **11**, DOI: 10.3390/mi11060603.

22. Tang, M., G. Wang, S.K. Kong, and H.P. Ho *A Review of Biomedical Centrifugal Microfluidic Platforms*. Micromachines, 2016. **7**, DOI: 10.3390/mi7020026.
23. Strohmeier, O., M. Keller, F. Schwemmer, S. Zehnle, D. Mark, F. von Stetten, R. Zengerle, and N. Paust *Centrifugal microfluidic platforms: advanced unit operations and applications*. Chemical Society Reviews, 2015. **44**, 6187-229 DOI: 10.1039/c4cs00371c.
24. Kong, L.X., A. Perebikovsky, J. Moebius, L. Kulinsky, and M. Madou *Lab-on-a-CD*. Journal of Laboratory Automation, 2016. **21**, 323-355 DOI: 10.1177/2211068215588456.
25. Aeinehvand, M.M., P. Magaña, M.S. Aeinehvand, O. Aguilar, M.J. Madou, and S.O. Martinez-Chapa *Ultra-rapid and low-cost fabrication of centrifugal microfluidic platforms with active mechanical valves*. RSC Advances, 2017. **7**, 55400-55407 DOI: 10.1039/c7ra11532f.
26. Aeinehvand, M.M., L. Weber, M. Jiménez, A. Palermo, M. Bauer, F.F. Loeffler, F. Ibrahim, F. Breitling, J. Korvink, M. Madou, D. Mager, and S.O. Martínez-Chapa *Elastic reversible valves on centrifugal microfluidic platforms*. Lab on a Chip, 2019. **19**, 1090-1100 DOI: 10.1039/C8LC00849C.
27. Hess, J.F., S. Zehnle, P. Juelg, T. Hutzenlaub, R. Zengerle, and N. Paust *Review on pneumatic operations in centrifugal microfluidics*. Lab on a Chip, 2019. **19**, 3745-3770 DOI: 10.1039/C9LC00441F.
28. Nguyen, H.V., V.D. Nguyen, H.Q. Nguyen, T.H.T. Chau, E.Y. Lee, and T.S. Seo *Nucleic acid diagnostics on the total integrated lab-on-a-disc for point-of-care testing*. Biosensors and Bioelectronics, 2019. **141**, 111466 DOI: 10.1016/j.bios.2019.111466.
29. Rombach, M., S. Hin, M. Specht, B. Johannsen, J. Lüddecke, N. Paust, R. Zengerle, L. Roux, T. Sutcliffe, J.R. Peham, C. Herz, M. Panning, O. Donoso Mantke, and K. Mitsakakis *RespiDisk: a point-of-care platform for fully automated detection of respiratory tract infection pathogens in clinical samples*. The Analyst, 2020. **145**, 7040-7047 DOI: 10.1039/d0an01226b.
30. Homann, A.R., L. Niebling, S. Zehnle, M. Beutler, L. Delamotte, M.-C. Rothmund, D. Czurratis, K.-D. Beller, R. Zengerle, H. Hoffmann, and N. Paust *A microfluidic cartridge for fast and accurate diagnosis of Mycobacterium tuberculosis infections on standard laboratory equipment*. Lab on a Chip, 2021. DOI: 10.1039/d1lc00035g.
31. Madadelahi, M., L.F. Acosta-Soto, S. Hosseini, S.O. Martinez-Chapa, and M.J. Madou *Mathematical modeling and computational analysis of centrifugal microfluidic platforms: a review*. Lab on a Chip, 2020. **20**, 1318-1357 DOI: 10.1039/c9lc00775j.
32. Miyazaki, C.M., E. Carthy, and D.J. Kinahan *Biosensing on the Centrifugal Microfluidic Lab-on-a-Disc Platform*. Processes, 2020. **8**, 1360 DOI: 10.3390/pr8111360.
33. Rombach, M., S. Hin, M. Specht, B. Johannsen, J. Lüddecke, N. Paust, R. Zengerle, L. Roux, T. Sutcliffe, J.R. Peham, C. Herz, M. Panning, O. Donoso Mantke, and K. Mitsakakis, *RespiDisk: a point-of-care platform for fully automated detection of respiratory tract infection pathogens in clinical samples.* The Analyst, 2020. **145**(21): p. 7040-7047.
34. Clime, L., J. Daoud, D. Brassard, L. Malic, M. Geissler, and T. Veres *Active pumping and control of flows in centrifugal microfluidics*. Microfluidics and Nanofluidics, 2019. **23**, DOI: 10.1007/s10404-019-2198-x.
35. Brassard, D., M. Geissler, M. Descarreaux, D. Tremblay, J. Daoud, L. Clime, M. Mounier, D. Charlebois, and T. Veres *Extraction of nucleic acids from blood: unveiling the potential of active pneumatic pumping in centrifugal microfluidics for integration and automation of sample preparation processes*. Lab on a Chip, 2019. **19**, 1941-1952 DOI: 10.1039/c9lc00276f.
36. Abi-Samra, K., R. Hanson, M. Madou, and R.A. Gorkin *Infrared controlled waxes for liquid handling and storage on a CD-microfluidic platform*. Lab on a Chip, 2011. **11**, 723-726 DOI: 10.1039/c0lc00160k.
37. Kong, L.X., K. Parate, K. Abi-Samra, and M. Madou *Multifunctional wax valves for liquid handling and incubation on a microfluidic CD*. Microfluidics and Nanofluidics, 2015. **18**, 1031-1037 DOI: 10.1007/s10404-014-1492-x.

38. Zehnle, S., F. Schwemmer, R. Bergmann, F. von Stetten, R. Zengerle, and N. Paust *Pneumatic siphon valving and switching in centrifugal microfluidics controlled by rotational frequency or rotational acceleration*. Microfluidics and Nanofluidics, 2015. **19**, 1259-1269 DOI: 10.1007/s10404-015-1634-9.
39. Ducrée, J. *Systematic review of centrifugal valving based on digital twin modelling towards highly integrated Lab-on-a-Disc systems*. Nature Microsystems & Nanoengineering, 2021.
40. Thorsen, T., *Microfluidic Large-Scale Integration.* Science, 2002. **298**(5593): p. 580-584.
41. Grieves, M. and J. Vickers, *Digital Twin: Mitigating Unpredictable, Undesirable Emergent Behavior in Complex Systems*, in *Transdisciplinary Perspectives on Complex Systems: New Findings and Approaches*, F.-J. Kahlen, S. Flumerfelt, and A. Alves, Editors. 2017, Springer International Publishing: Cham. p. 85-113.
42. Ducrée, J. *Secure air traffic control at the hub of multiplexing on the centrifugo-pneumatic Lab-on-a-Disc platform*. Micromachines, 2021. DOI: 10.20944/preprints202104.0612.v1.
43. Ducrée, J. *Efficient development of integrated Lab-On-A-Chip systems featuring operational robustness and nanufacturability*. Micromachines, 2019. **10**, 12 DOI: 10.3390/mi10120886.
44. Reyes, D.R., H.v. Heeren, S. Guha, L.H. Herbertson, A.P. Tzannis, J. Ducrée, H. Bissig, and H. Becker *Accelerating Innovation and Commercialization Through Standardization of Microfluidic-Based Medical Devices*. Lab on a Chip, 2021. DOI: 10.1039/D0LC00963F.
45. Mark, D., S. Haeberle, T. Metz, S. Lutz, J. Ducrée, R. Zengerle, and F. von Stetten *Aliquoting structure for centrifugal microfluidics based on a new pneumatic valve*. MEMS 2008: 21st Ieee International Conference on Micro Electro Mechanical Systems, Technical Digest, 2008. 611-+.
46. Schwemmer, F., T. Hutzenlaub, D. Buselmeier, N. Paust, F. von Stetten, D. Mark, R. Zengerle, and D. Kosse *Centrifugo-pneumatic multi-liquid aliquoting-parallel aliquoting and combination of multiple liquids in centrifugal microfluidics*. Lab on a Chip, 2015. **15**, 3250-3258 DOI: 10.1039/c5lc00513b.
47. Keller, M., S. Wadle, N. Paust, L. Dreesen, C. Nuese, O. Strohmeier, R. Zengerle, and F. von Stetten *Centrifugo-thermopneumatic fluid control for valving and aliquoting applied to multiplex real-time PCR on off-the-shelf centrifugal thermocycler*. RSC Advances, 2015. **5**, 89603-89611 DOI: 10.1039/c5ra16095b.
48. Grumann, M., A. Geipel, L. Riegger, R. Zengerle, and J. Ducrée *Batch-mode mixing on centrifugal microfluidic platforms*. Lab on a Chip, 2005. **5**, 560-5 DOI: 10.1039/b418253g.
49. Ducrée, J., T. Brenner, S. Haeberle, T. Glatzel, and R. Zengerle *Multilamination of flows in planar networks of rotating microchannels*. Microfluidics and Nanofluidics, 2006. **2**, 78-84 DOI: 10.1007/s10404-005-0056-5.
50. Burger, R.K., David; Cayron, Hélène ; Reis, Nuno ; Garcia da Fonseca, João;Ducrée, Jens *Siphon-induced droplet break-off for enhanced mixing on a centrifugal platform*. Inventions, 2020. **5**, DOI: 10.3390/inventions5010001.
51. Ducrée, J., S. Haeberle, T. Brenner, T. Glatzel, and R. Zengerle *Patterning of flow and mixing in rotating radial microchannels*. Microfluidics and Nanofluidics, 2006. **2**, 97-105 DOI: 10.1007/s10404-005-0049-4.
52. Strohmeier, O., S. Keil, B. Kanat, P. Patel, M. Niedrig, M. Weidmann, F. Hufert, J. Drexler, R. Zengerle, and F. von Stetten *Automated nucleic acid extraction from whole blood, B. subtilis, E. coli, and Rift Valley fever virus on a centrifugal microfluidic LabDisk*. RSC Advances, 2015. **5**, 32144-32150 DOI: 10.1039/c5ra03399c.
53. Karle, M., J. Miwa, G. Roth, R. Zengerle, and F. von Stetten *A Novel Microfluidic Platform for Continuous DNA Extraction and Purification Using Laminar Flow Magnetophoresis*. IEEE 22nd International Conference on Micro Electro Mechanical Systems (MEMS 2009), 2009. 276-279 DOI: 10.1109/Memsys.2009.4805372.

54. Kido, H., M. Micic, D. Smith, J. Zoval, J. Norton, and M. Madou *A novel, compact disk-like centrifugal microfluidics system for cell lysis and sample homogenization*. Colloids and Surfaces B-Biointerfaces, 2007. **58**, 44-51 DOI: 10.1016/j.colsurfb.2007.03.015.
55. Haeberle, S., T. Brenner, R. Zengerle, and J. Ducrée *Centrifugal extraction of plasma from whole blood on a rotating disk*. Lab on a Chip, 2006. **6**, 776-781 DOI: 10.1039/b604145k.
56. Steigert, J., T. Brenner, M. Grumann, L. Riegger, S. Lutz, R. Zengerle, and J. Ducrée *Integrated siphon-based metering and sedimentation of whole blood on a hydrophilic lab-on-a-disk*. Biomedical Microdevices, 2007. **9**, 675-679 DOI: 10.1007/s10544-007-9076-0.
57. Kinahan, D.J., S.M. Kearney, N.A. Kilcawley, P.L. Early, M.T. Glynn, and J. Ducrée *Density-Gradient Mediated Band Extraction of Leukocytes from Whole Blood Using Centrifugo-Pneumatic Siphon Valving on Centrifugal Microfluidic Discs*. PLOS ONE, 2016. **11**, e0155545 DOI: 10.1371/journal.pone.0155545.
58. Dimov, N., J. Gaughran, D. Mc Auley, D. Boyle, D.J. Kinahan, and J. Ducrée, *Centrifugally Automated Solid-Phase Purification of RNA*, in *2014 IEEE 27th International Conference on Micro Electro Mechanical Systems (MEMS)*. 2014: Cancun, Mexico. p. 260-263 DOI: 10.1109/MEMSYS.2014.6765625.
59. Gaughran, J., D. Boyle, J. Murphy, R. Kelly, and J. Ducrée *Phase-selective graphene oxide membranes for advanced microfluidic flow control*. Microsystems and Nanoengineering, 2016. **2**, 16008 DOI: 10.1038/micronano.2016.8.
60. Haeberle, S., R. Zengerle, and J. Ducrée *Centrifugal generation and manipulation of droplet emulsions*. Microfluidics and Nanofluidics, 2007. **3**, 65-75 DOI: 10.1007/s10404-006-0106-7.
61. Schuler, F., F. Schwemmer, M. Trotter, S. Wadle, R. Zengerle, F. von Stetten, and N. Paust *Centrifugal step emulsification applied for absolute quantification of nucleic acids by digital droplet RPA*. Lab on a Chip, 2015. **15**, 2759-2766 DOI: 10.1039/c5lc00291e.
62. Schuler, F., M. Trotter, M. Geltman, F. Schwemmer, S. Wadle, E. Dominguez-Garrido, M. Lopez, C. Cervera-Acedo, P. Santibanez, F. von Stetten, R. Zengerle, and N. Paust *Digital droplet PCR on disk*. Lab on a Chip, 2016. **16**, 208-216 DOI: 10.1039/c5lc01068c.
63. Ducrée, J. *Efficient Development of Microfluidic Solutions for Bioanalytical "Point-of-Use" Testing towards High-Technology-Readiness Levels—A Platform-Based Design-for-Manufacture Approach*. Proceedings, 2019. **2**, DOI: 10.3390/proceedings2131097.
64. Ducrée, J., M. Etzrodt, S. Bartling, R. Walshe, T. Harrington, N. Wittek, S. Posth, K. Wittek, A. Ionita, W. Prinz, and J. Lawton *Unchaining Collective Intelligence for Science, Research and Technology Development by Blockchain-Boosted Community Participation*. Frontiers in Blockchain, 2020. **4**, 631648 DOI: 10.3389/fbloc.2021.631648.
65. Ducrée, J. *Research – A blockchain of knowledge?* Blockchain: Research and Applications, 2020. **1**, 100005 DOI: 10.1016/j.bcra.2020.100005.
66. Ducrée, J., M. Gravitt, R. Walshe, S. Bartling, M. Etzrodt, and T. Harrington *Open Platform Concept for Blockchain-Enabled Crowdsourcing of Technology Development and Supply Chains*. Frontiers in Blockchain, 2020. **3**, 386525 DOI: 10.3389/fbloc.2020.586525.
67. Ducrée, J., M. Etzrodt, B. Gordijn, M. Gravitt, S. Bartling, R. Walshe, and T. Harrington *Blockchain for Organising Effective Grass-Roots Actions on a Global Commons: Saving The Planet*. Frontiers in Blockchain, 2020. **3**, 33 DOI: 10.3389/fbloc.2020.00033.